

PROCEEDINGS OF SPIE

SPIDigitalLibrary.org/conference-proceedings-of-spie

Wide-field optical properties estimation of whole limbs in muscle dystrophy murine models via SFDI: a case study

Verónica Mieites, José Gutiérrez-Gutiérrez, Arturo Pardo, Xavier Suárez-Calvet, José Miguel López-Higuera, et al.

Verónica Mieites, José A. Gutiérrez-Gutiérrez, Arturo Pardo, Xavier Suárez-Calvet, José Miguel López-Higuera, Jordi Díaz-Manera, Olga M. Conde, "Wide-field optical properties estimation of whole limbs in muscle dystrophy murine models via SFDI: a case study," Proc. SPIE 12627, Translational Biophotonics: Diagnostics and Therapeutics III, 1262731 (11 August 2023); doi: 10.1117/12.2670573

SPIE.

Event: European Conferences on Biomedical Optics, 2023, Munich, Germany

Wide-field optical properties estimation of whole limbs in muscle dystrophy murine models via SFDI: a case study

Verónica Mieites^{a,b}, José A. Gutiérrez-Gutiérrez^{a,b}, Arturo Pardo^a, Xavier Suárez-Calvet^{c,d}, José Miguel López-Higuera^{a,b,e}, Jordi Díaz-Manera^{c,d,f}, and Olga M. Conde^{a,b,e}

^aGrupo de Ingeniería Fotónica, Dep. TEISA, Universidad de Cantabria (Avda. Los Castros S/N, 39006, Santander, Spain)

^bInstituto de Investigación Sanitaria Valdecilla (IDIVAL) (C. Cardenal Herrera Oria, 39011, Santander, Spain)

^cInstituto de Investigación Biomédica del Hospital de la Santa Creu Sant Pau (Carrer de Sant Antoni Maria Claret, 167, 08025 Barcelona, Spain)

^dCIBER-ER (C. de Melchor Fernández Almagarro, 3, 28029, Madrid, Spain)

^eCIBER-BBN (C. de Melchor Fernández Almagarro, 3, 28029, Madrid, Spain)

^fJohn Walton Muscular Dystrophy Research Centre, University of Newcastle (Newcastle upon Tyne NE1 7RU, UK)

ABSTRACT

This manuscript analyzes the optical properties of dystrophic mice legs, which have been obtained by Spatial Frequency Domain Imaging (SFDI). We used a custom-built SFDI system with spectrometric capabilities so that wavelength-resolved absorption (μ_a) and scattering (μ'_s) coefficients can be calculated. Samples were measured sequentially at ten different frequencies to find their frequency-dependent diffuse reflectance. Additionally, the Monte Carlo method has been applied to generate a Look-Up Table (LUT) to speed up the estimation of the optical parameters, with the GPU-accelerated version of Monte Carlo for Multi-Layered tissues (MCML), CUDAMCML. We found that the diffuse reflectance (R_d) has a different behavior in terms of the wavelength (λ), which gave rise to different values of μ_a and μ'_s in terms of λ . Given that the μ_a is related to the chemical composition, the differences in wavelength could be used to quantify the presence of chemical components in the samples and, the μ'_s , which relates to the internal structure, can be utilized to identify dystrophy centers inside the mice leg.

Keywords: SFDI, mice models, Monte Carlo, diffusion, muscular dystrophy.

1. INTRODUCTION

Optical properties can be used as non-invasive tools to analyze samples without damaging tissues, which is especially useful when dealing with biological tissues, where samples are scarce and delicate. Rare diseases, such as muscular dystrophies, have low presence in the population, which means that most research efforts are not applied to such specific fields. The main method of examination in the case of muscular dystrophies is one or more muscular biopsies, followed by histological tests. In order to analyze samples, they have to be cut in a number of sections that need to be individually examined, making dystrophic samples hard-to-access, one-time-use samples.

Spatial Frequency Domain Imaging (SFDI) is a well-known, mature, wide-field optical imaging technique that does not require sample preprocessing, so it can be applied, *ex vivo* or *in vivo*, to obtain optical parameters related to the chemical (absorption coefficient μ_a) and structural (reduced scattering coefficient μ'_s) components inside a sample.¹ This technique is based on projecting a pattern of fringes, with different spatial frequencies (f_x), and measuring the Modulation Transfer Function (MTF), so that the diffuse reflectance at those frequencies

Further author information: (Send correspondence to V.M.A.)

V.M.A.: E-mail: veronica.mieites@unican.es

O.C.P.: E-mail: olga.conde@unican.es

Translational Biophotonics: Diagnostics and Therapeutics III, edited by
Zhiwei Huang, Lothar D. Ilige, Proc. of SPIE Vol. 12627, 1262731
© 2023 SPIE · 0277-786X · doi: 10.1117/12.2670573

(R_d) can be obtained. By using either analytical expressions or Monte-Carlo-based simulations, the measured R_d can be related to both μ_a and μ'_s .

In this work, we propose the use of a custom-built hyperspectral SFDI system to obtain both the absorption and scattering signatures of dystrophic mice legs to define how they behave when the disease is active. Since our device is combined with a Hyper-Spectral Imaging (HSI) system that allows us to obtain the reflectance at various wavelengths (λ), we present the behavior of μ_a and μ'_s across multiple λ values to further discuss the use of SFDI as a non-invasive histology alternative to analyze dystrophic mice samples.

2. MATERIALS AND METHODS

SFDI system. Our SFDI system was built on top of our previously described HSI device.² The HSI contains a line spectrometer that decomposes the spectra onto a camera sensor and uses a rotating mirror to scan the whole sample. To get the SFDI capabilities, we added a projector that illuminates the sample with the frequency patterns. The whole system³ provides us with a spatial resolution of $250\mu m$ and a wavelength resolution of $3nm$, for wavelengths between $400nm$ and $1000nm$.

Samples. We used three *ex vivo* dystrophic mouse legs, since we wanted to perform full-limb measurements to test our approach. The legs conserve both muscles and skin, so that they could be used to simulate *in vivo* experiments. Samples are extracted and prepared at the Neuromuscular Diseases Unit (Hospital de la Santa Creu I Sant Pau, Univ. Autònoma de Barcelona) and measured at the Photonics Engineering Group (Univ. Cantabria).

Measurements. We measured the legs at 12 different spatial frequencies (f_x), where the two smallest ones were used to extract the samples profilometry. Specifically, we used the following values: $f_x = [0.05, 0.1, 0.11, 0.22, 0.334, 0.44, 0.56, 0.67, 0.78, 0.89, 1.0] mm^{-1}$. As explained further below, each SFDI frequency is required to be measured at three different phases (ϕ_1, ϕ_2, ϕ_3) in order to obtain the MTF. Given that a single measurement took about 9 minutes, the whole range of frequencies was measured over 4.5 hours, which would make such specific measurements very unpractical in *in vivo* scenarios. Fortunately, the samples only need to be characterized once, therefore after the most relevant frequencies and wavelengths are identified, any future experiment could focus on measuring only a reduced set of them.

Analysis: Optical properties. The measurement and analysis methods used in SFDI were first introduced by Cuccia *et al* in 2009 and the full derivations are included in their paper⁴ as follows. Let I be the projected intensity values on a sample, modulated as a cosine of spatial frequency f_x as

$$I(f_x) = \frac{I_0}{2} [1 + \cos(2\pi f_x x + \phi)] \quad (1)$$

where I_0 is the intensity of the source, ϕ is the spatial phase offset and x is the spatial point. By choosing three different illumination offsets (ϕ_1, ϕ_2, ϕ_3) that create three different patterns (I_1, I_2, I_3), we obtained the diffuse reflectance as a function of x and f_x , $R_d(x, f_x)$, as

$$R_d(x, f_x) = \frac{M_{AC}(x, f_x)}{M_{AC,ref}(x, f_x)} \cdot R_{d,ref}(f_x) \quad (2)$$

where M_{AC} is the envelope of the diffuse-reflected photon density (calculated with I_1, I_2 and I_3) and the subindex *ref* denotes the parameters which are calculated via measurements of a reference material which, in this case, was a Spectralon disk of known optical properties and thickness $2.66 \pm 0.02mm$. To properly extract the optical properties, we modified the $M_{AC,ref}$ with the samples profilometry⁵ by first obtaining calibration curves that describe how a non-flat surface alters the cosines projections,

Once the diffuse reflectance is obtained, it can be related to the absorption (μ_a) and the reduced scattering (μ'_s) coefficients of the sample by applying the diffusion approximation ($\mu'_s \gg \mu_a$) to the radiative transfer

equation and using the resultant expression to fit the data, or by using the Monte Carlo method to simulate the reflected photon packets. We chose the latter to create a Look-Up-Table (LUT) of 100×100 sets of μ'_s and μ_a to explore a wide-range of possible tissue parameters. By having a pre-calculated LUT, the comparison of the samples $R_d(f_x)$ with the reflectance values inside the LUT is much faster⁶ than fitting them, point-by-point, to an analytical expression. For the Monte Carlo (MC) implementation, we used CUDAMCML,⁷ which is a GPU-accelerated version of the commonly used Monte Carlo for Multi-Layered tissues (MCML).⁸ We also applied CUDAMCML to simulate $R_{d,ref}(f_x)$ at different wavelengths.⁹

3. RESULTS AND DISCUSSION

We measured three dystrophic mice legs at ten different spatial frequencies (f_x) for each of the wavelengths of our light source (λ) and calculated their diffuse reflectance, $R_d(f_x, \lambda)$ for each point in the sample. Figure 1 contains the results for one representative sample. In figure 1a we show the average reflectance obtained for the whole wavelength range (423-662nm) and for the blue (450-490nm), green (530-570nm) and red (645-662nm) color ranges. Generally speaking, we found the main drop in reflectance between $f_x = 0.0mm^{-1}$ and $f_x = 0.11mm^{-1}$, followed by a slowly decreasing slope, indicating a steep MTF for the mice legs. Higher reflectancies were measured for the reds, then the blues, which always yielded similar values to the overall average, and finally, the greens. In the case of the reds, we observed a slight increase in the R_d from $f_x = 0.11mm^{-1}$ onwards, which could mean a different interaction of the samples with the projected light in this specific wavelength range. Even though this behavior was repeated across the three samples, it should be noted that the reds range has the fewer number of wavelengths in the average, due to our light source limitations. Furthermore, the Spectralon reference (fig. 1b) has greater wavelength dispersion as the frequency increases, which could be exaggerating the difference in slopes as f_x grows.

The examination area of the legs measured was, approximately, 2.5cm wide, 3cm long and 1.5cm thick, so we had to perform profilometry to obtain the reflectance (fig. 1c). Even though the legs were properly corrected, some areas (i.e., the right side of the images) show a decrease in reflectance that can be caused by the decreased signal-to-noise ratio (SNR) that happens in lower regions of the sample. SNR was already low due to the chosen exposure time (300ms) to keep the measurements as fast as possible, which makes the extraction of optical properties in lower SNR areas or darker regions in the samples (i.e., hair) especially challenging.

Regarding the absorption (fig. 1d) we found that, on average, μ_a increased the textural information, given that it highlights different regions than μ'_s and R_d , which share more similarities. The values of μ_a varied slightly across the wavelengths (fig. 1f, top), with the less spread values in the red wavelengths range and those in the greens range being saturated. To properly quantify the data in this color range, we will perform more simulations with greater upper limit for μ_a . Regardless, the differences in absorption indicate a different chemical composition, which could be used to quantify the components when taking into account the wavelength-dependent behavior. Regarding the scattering (fig. 1e), the samples appeared more homogeneous, with less drastic changes than the μ_a , as verified by its histogram across wavelengths (fig. 1f, bottom). Moreover, each μ'_s range occupied an independent distribution, which could be useful to perform image segmentation, in terms of wavelength, to have μ'_s images that point to different structures inside the sample. The values of μ_a we found are in good accordance with the bibliography (on average, $\mu_a \approx (1, 2)mm^{-1}$ for male and female mice¹⁰), but our values of μ'_s are lower than those previously reported (on average, $\mu'_s \approx (10, 20)mm^{-1}$ for male and female mice¹⁰), which could be an indicator of the structural changes suffered in dystrophic mice.

4. CONCLUSIONS

We used a custom-built hyperspectral SFDI system to analyze three dystrophic mice legs and obtain their optical properties. By measuring the samples at ten different spatial frequencies f_x , at wavelengths λ between 423nm and 662nm, we obtained the diffuse reflectance R_d for each point in the samples. We found that the R_d has an initial drop, followed by a slower decrease, except in the case of the reds, where the R_d increments slightly.

By comparing the $R_d(f_x, \lambda)$ with the values inside the pre-calculated LUT, we found the absorption μ_a and reduced scattering μ'_s coefficients. Both magnitudes have different behavior with λ , which could make them

useful to quantify the molecular components of the samples (in the case of μ_a) and to estimate the degree of dystrophy (by using μ'_s).

Even though all of the results presented in this manuscript arose from a reduced sample size of three mice legs and are preliminary, the repeatability we saw between samples is a good indicator that hyperspectral-SFDI can be a powerful tool to evaluate optical properties related to the chemical and structural composition of samples without modifying them in the process.

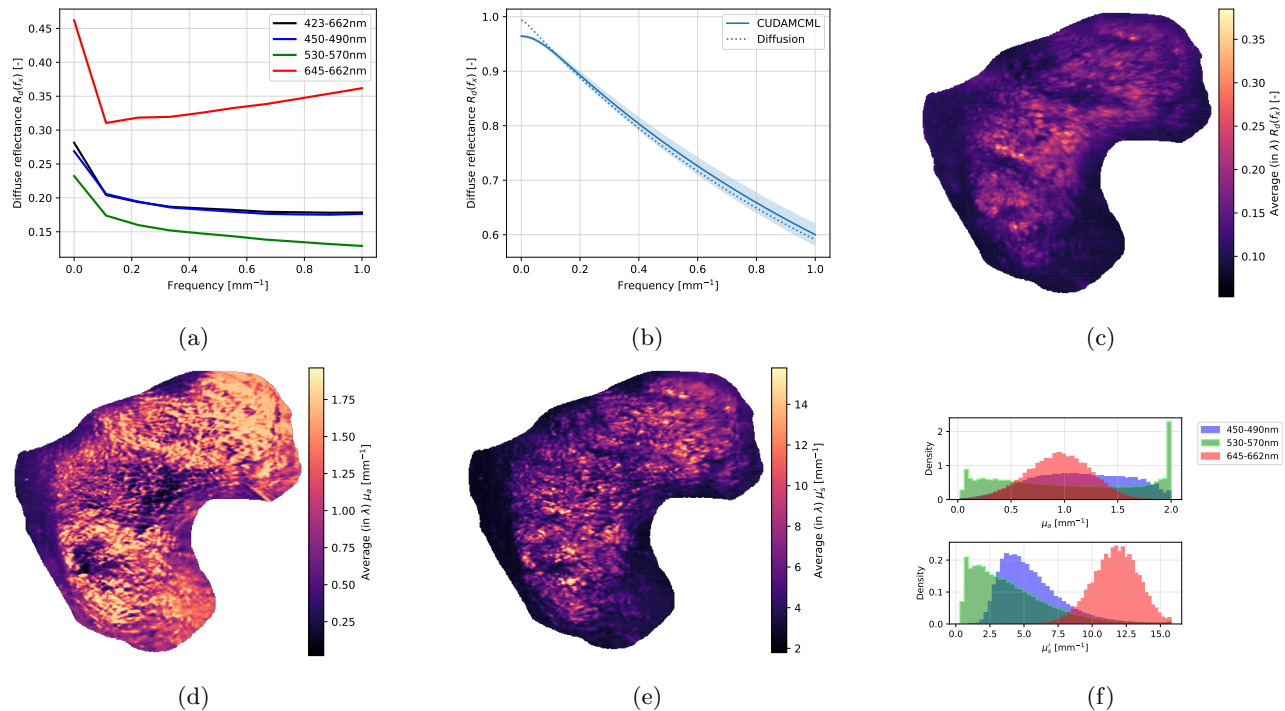


Figure 1: (a) Average R_d obtained through the LUT in the whole wavelength range (black), for the 450-490nm range (blue), for the 530-570nm range (green) and for the 645-662nm range (red). (b) Average R_d , across wavelengths, as obtained by CUDAMCML (dashed line) and the diffusion approximation (solid line), with the wavelength standard variation as the colored area. (c) Average diffuse reflectance across all wavelengths for one of the mice legs. Image of the average absorption and reduced scattering coefficients across all wavelengths (d and e). Histograms of the average μ_a (top) and μ'_s (bottom) in the three color ranges (f).

Acknowledgements

Support for this work was provided by the projects PREVAL 21/07 (FUSIOMUSCLE), SUBVTC-2021-0038 (HYPER-fusionTRANS), EQC 2019-006589-P, DTS22-00127(hyPERfusioCAM), DTS17-00055 (INTRACARDIO) and DISFOS (PID2019-107270RB-C21/AEI/ 10.13039/ 501100011033), financed by the ISCIII, the Fundación Instituto de Investigación Valdecilla (IDIVAL) and the Spanish Ministry of Science, Innovation and Universities, co-financed with FEDER funds.

REFERENCES

- [1] S. Gioux, A. Mazhar, and D. J. Cuccia, "Spatial frequency domain imaging in 2019: principles, applications, and perspectives," *J Biomed Opt*, vol. 24, no. 7, pp. 1–18, Jun. 2019.
- [2] J. A. Gutiérrez-Gutiérrez, A. Pardo, E. Real, J. M. López-Higuera, and O. M. Conde, "Custom scanning hyperspectral imaging system for biomedical applications: Modeling, benchmarking, and specifications," *Sensors*, vol. 19, no. 7, 2019. [Online]. Available: <https://doi.org/10.3390/s19071692>

- [3] A. Pardo Franco, "Light, machines, and cancer: Imaging systems and processing techniques for wide-field diagnostics in scattering media," Ph.D. dissertation, Universidad de Cantabria, 6 2022. [Online]. Available: <https://hdl.handle.net/10902/26190>
- [4] D. J. Cuccia, F. Bevilacqua, A. J. Durkin, F. R. Ayers, and B. J. Tromberg, "Quantitation and mapping of tissue optical properties using modulated imaging," *J Biomed Opt*, vol. 14, no. 2, p. 024012, Mar. 2009. [Online]. Available: <https://doi.org/10.1117/1.3088140>
- [5] S. Gioux, A. Mazhar, D. J. Cuccia, A. J. Durkin, B. J. Tromberg, and J. V. Frangioni, "Three-dimensional surface profile intensity correction for spatially modulated imaging," *J Biomed Opt*, vol. 14, no. 3, p. 034045, May 2009. [Online]. Available: <https://doi.org/10.1117/1.3156840>
- [6] S. Panigrahi and S. Gioux, "Machine learning approach for rapid and accurate estimation of optical properties using spatial frequency domain imaging," *J Biomed Opt*, vol. 24, no. 7, pp. 1–6, Dec. 2018. [Online]. Available: <https://doi.org/10.1117/1.JBO.24.7.071606>
- [7] E. Alerstam, T. Svensson, and S. Andersson-Engels, "Parallel computing with graphics processing units for high-speed Monte Carlo simulation of photon migration," *Journal of Biomedical Optics*, vol. 13, no. 6, p. 060504, 2008. [Online]. Available: <https://doi.org/10.1117/1.3041496>
- [8] L. Wang, S. L. Jacques, and L. Zheng, "Mcmcl—monte carlo modeling of light transport in multi-layered tissues," *Computer Methods and Programs in Biomedicine*, vol. 47, no. 2, pp. 131–146, 1995. [Online]. Available: [https://doi.org/10.1016/0169-2607\(95\)01640-F](https://doi.org/10.1016/0169-2607(95)01640-F)
- [9] D. Khoptyar, A. A. Subash, S. Johansson, M. Saleem, A. Sparén, J. Johansson, and S. Andersson-Engels, "Broadband photon time-of-flight spectroscopy of pharmaceuticals and highly scattering plastics in the vis and close nir spectral ranges," *Opt. Express*, vol. 21, no. 18, pp. 20941–20953, Sep 2013. [Online]. Available: <https://opg.optica.org/oe/abstract.cfm?URI=oe-21-18-20941>
- [10] K. Calabro, A. Curtis, J.-R. Galarneau, T. Krucker, and I. J. Bigio, "Gender variations in the optical properties of skin in murine animal models," *J Biomed Opt*, vol. 16, no. 1, p. 011008, Jan. 2011. [Online]. Available: <https://doi.org/10.1117/1.3525565>
- [11] S. L. Jacques, "Optical properties of biological tissues: a review," *Phys Med Biol*, vol. 58, no. 11, pp. R37–61, May 2013.